Theoretical and experimental signal-to-noise ratio assessment in new direction sensing continuous-wave Doppler lidar

Pedersen, Anders Tegtmeier; Foroughi Abari, Farzad; Mann, Jakob; Mikkelsen, Torben

Published in:
Journal of Physics: Conference Series (Online)

Link to article, DOI:
10.1088/1742-6596/524/1/012004

Publication date:
2014

Document Version
Publisher's PDF, also known as Version of record

Theoretical and experimental signal-to-noise ratio assessment in new direction sensing continuous-wave Doppler lidar

2014 J. Phys.: Conf. Ser. 524 012004

(http://iopscience.iop.org/1742-6596/524/1/012004)

Theoretical and experimental signal-to-noise ratio assessment in new direction sensing continuous-wave Doppler lidar

A Tegtmeier Pedersen, C F Abari, J Mann and T Mikkelsen

Department of Wind Energy, Technical University of Denmark, Frederiksborgvej 399, 4000 Roskilde, Denmark

E-mail: antp@dtu.dk

Abstract. A new direction sensing continuous-wave Doppler lidar based on an image-reject homodyne receiver has recently been demonstrated at DTU Wind Energy, Technical University of Denmark. In this contribution we analyse the signal-to-noise ratio resulting from two different data processing methods both leading to the direction sensing capability. It is found that using the auto spectrum of the complex signal to determine the wind speed leads to a signal-to-noise ratio equivalent to that of a standard self-heterodyne receiver. Using the imaginary part of the cross spectrum to estimate the Doppler shift has the benefit of a zero-mean background spectrum, but comes at the expense of a decrease in the signal-to noise ratio by a factor of $\sqrt{2}$.

1. Introduction

Coherent Doppler lidars have in recent years started to play an increasingly important role within the wind energy industry and are now widely used for especially resource assessment. Lidars offer a cost-efficient and flexible alternative to in-situ anemometers, and met masts and several commercial products have found their way to the market. Despite being a well-established technology coherent Doppler lidars still represent a very active research field both in terms of the instruments themselves and their applications. Critical parameters such as accuracy and maximum measurement range are constantly being improved, and new features like controllable scanning patterns are emerging. For the application of lidars in wind energy the lidars seem to be moving from the ground to being mounted directly on the turbine, and e.g. power curve measurements from turbine mounted lidars have been demonstrated [1]. Another interesting application relates to turbine control where the aim is to maximise energy production and turbine lifetime through feed-forward yaw and pitch control using a turbine mounted lidar [2].

1.1. Direction sensing continuous-wave lidar

Continuous-wave (CW) Doppler wind lidars possess several desirable properties such as a simple basic design and a high duty cycle measuring rate, but unfortunately also some less desirable features such as limited measuring range and missing capability of sensing the direction of the wind. One can work around the latter limitation by shifting the frequency of the reference local oscillator (LO) compared to the transmitted signal, e.g. with the aid of an acousto-optic modulator (AOM). However, this approach has shown to lead to practical problems with

instabilities in the Doppler spectrum especially at frequencies close to the acoustic frequency of the AOM and to effectively limit the bandwidth.

At DTU Wind Energy a different technique to achieve direction sensing has recently been demonstrated with great success [3]. This detection scheme is based on an image-reject homodyne receiver, also known as coherent in-phase and quadrature (IQ) detection, which in essence works by dividing the received backscattered signal in two and mixing one half with a reference local oscillator signal and the other half with a 90° delayed copy of the LO [4, 5]. By calculating the cross spectrum between these two signals the sign of the Doppler shift and thus the direction of the wind can be deduced. The cross spectrum between the two channels furthermore has the advantage of automatically eliminating any DC component and background noise contributions thus making noise flattening obsolete in the post processing. In this study we analyse the signal-to-noise ratio (SNR) of the IQ detection lidar theoretically and experimentally, and compare with that of a lidar detection system using the standard self-heterodyne technique.

1.2. Experimental setup

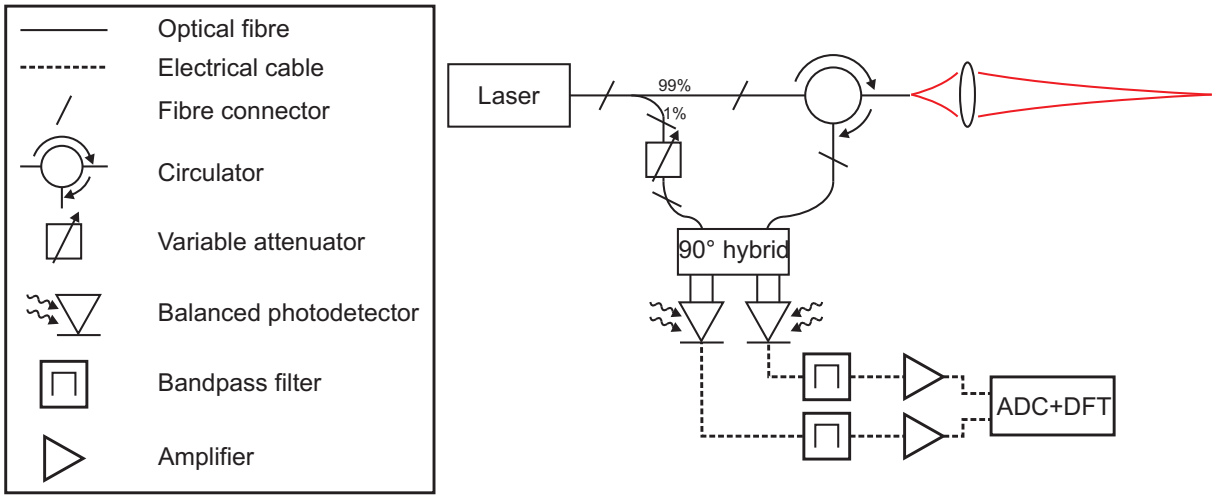

Figure 1. Schematic drawing of the direction sensing lidar used in this study.

Figure 1 shows a sketch of the setup for the direction sensing CW lidar used in this study. A 1565 nm CW fibre laser delivers an output power of approximately 1 W. This is sent to an optical circulator and from there to the telescope unit which focuses the light into the atmosphere. Light scattered back into the same mode as the output is collected by the telescope and directed back to the circulator and from here to the 90°-hybrid. Here the backscattered signal is mixed with the local oscillator signal (LO) which is tapped out from the laser output using a 1/99 optical splitter. The hybrid splits the received signal and the LO in two and introduces a 90° phase shift on one of the two LO signals before they are mixed on two balanced photodetectors. In order to achieve an appropriate optical power level on the detectors the LO can be attenuated before entering the hybrid. The two analog electrical detector output signals are bandpass filtered to condition them and avoid aliasing before they are amplified and finally digitised and processed by an FPGA board and a computer.

1.3. Data processing

Due to the phase shift induced by the 90° hybrid the photocurrents generated by the two photodetectors are 90° out of phase and may thus be written as

$$i(t) \propto \sin(\omega_D t + \phi) \quad (1)$$
$$q(t) \propto \pm\cos(\omega_D t + \phi), \quad (2)$$

where $i(t)$ and $q(t)$ are called the in-phase and quadrature-phase signal, respectively, and the sign of $q(t)$ depends on the sign of the wind velocity. ω_D is here the Doppler shift frequency and ϕ is an arbitrary phase constant.

The signals may be processed in three different ways. The first of these is the standard auto spectrum, S_I, of each signal which can be calculated according to

$$S_I(\omega) = \left\langle |I(\omega)|^2 \right\rangle = \left\langle |\mathcal{F}\{i(t)\}|^2 \right\rangle, \quad (3)$$

in the case of the in-phase signal. Here $\mathcal{F}\{\cdot\}$ denotes the Fourier transform, and$\langle\rangle$ the ensemble average.

The auto spectra of both i and q are symmetric, i.e. the positive and negative halves of the spectra are identical, and can therefore not be used directly to determine the direction of the wind. One way to achieve this is instead to calculate the auto spectrum of the complex signal, S_C, defined as

$$S_C(\omega) = \left\langle |I(\omega) + jQ(\omega)|^2 \right\rangle = \left\langle |\mathcal{F}\{i(t) + jq(t)\}|^2 \right\rangle, \quad (4)$$

where $j = \sqrt{-1}$ is the complex unit. This operation results in a spectrum in which the image component of the Doppler peak is eliminated. That is, the Doppler peak will only be present in either the positive or the negative half of the spectrum depending on the sign of the Doppler shift, see Figure 2(a).

In the third data processing method the imaginary part of the cross spectrum, χ, between the two signals is used, i.e.

$$\Im(\chi(\omega)) = \langle \Im(I(\omega)Q^*(\omega)) \rangle = \langle \Im(\mathcal{F}\{i(t)\}\mathcal{F}^*\{q(t)\}) \rangle, \quad (5)$$

where $*$ denotes the complex conjugate and $\Im$ the imaginary part. This results in an anti-symmetric spectrum where the sign of the wind speed can be deduced from the sign of the Doppler peak, see Figure 2(b).

Figure 2 shows measured examples of the latter two methods described above. As can be seen the auto spectrum of the complex signal has a Doppler peak located around -2 MHz which for this specific lidar system is equivalent to a wind speed of approximately -1.5 m/s. The shape of the background spectrum is determined by the combined frequency response of the detectors, bandpass filters, and amplifiers. For example can the effect of the lowpass edge of the filters clearly be seen to set in at ± 50 MHz. A strong DC component is also present and this is probably due to a slight offset in the ADC or an imbalance in the optical part of the system, or stray light due to reflections from optical components such as the telescope. The same information, i.e. wind speed and direction, can be deduced from the imaginary part of the cross spectrum where the negative peak indicates a negative wind speed. With this method the negative half of the spectrum thus becomes obsolete which can be advantageous when storing spectra. Another advantage of using the cross spectrum, as can be seen from the figure, is the zero-mean flat background noise spectrum. As a result it is not necessary to first measure the noise spectrum in order to normalise the spectrum [6].

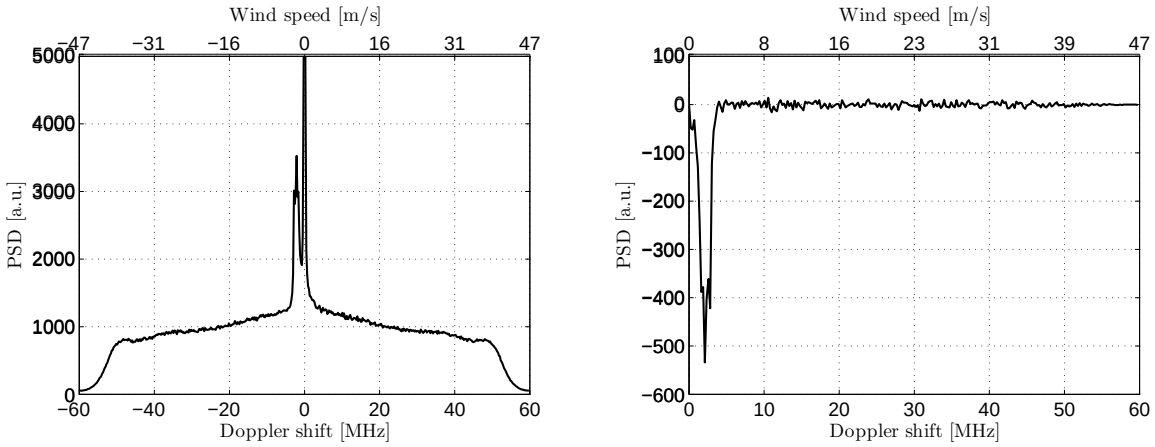

Figure 2. (a) Auto spectrum of the complex signal, Eq. (4). (b) Imaginary part of cross spectrum, Eq. (5).

2. Signal-to-noise ratio

In this section we will calculate the relative signal-to-noise ratios of the three data processing methods described above. In the following we will assume spectra with equal noise statistics across the full bandwidth, i.e. the standard deviation of the noise is the same in all frequency bins. For convenience and since we will be working solely in the frequency domain the angular frequency, ω, will be omitted in the equations.

2.1. Auto spectrum of individual signals

The auto spectrum of either I or Q is

$$\langle |I|^2 \rangle = \langle |Q|^2 \rangle = \begin{cases} S+N & \text{at Doppler peak} \\ N & \text{outside Doppler peak,} \end{cases} \tag{6}$$

where S and N are the power spectral density of the signal and of the background noise, respectively. When performing actual measurements we do not have access to the ensemble average but rather the average of a number n of spectra, which is typically of the order of a few hundreds to a few thousands. We denote that average by $\langle\rangle_n$. So, for example, $\langle |I|^2 \rangle_n = \frac{1}{n}\left(|I_1|^2 + |I_2|^2 + \ldots + |I_n|^2\right)$, where I_k is the k^{th} element from a series of consecutive Fourier amplitudes produced from a detector time series. It is reasonable to assume that I_k and I_l are independent (for $k \neq l$) for frequencies outside the Doppler peak, and also that the noise from the in-phase, I, and quadrature-phase, Q, signals are independent.

We now define the signal-to-noise ratio (SNR) as the signal power, i.e. how far the Doppler peak is above the noise floor, divided by the standard deviation of the noise level. So, for one of the detector signals, say I, the ratio is

$$\text{SNR} = \frac{(S+N) - N}{\sigma_n(N)} = \sqrt{n} S/N \equiv \text{SNR}_0, \tag{7}$$

where

$$\sigma_n^2(N) = \left\langle \left(\langle |I|^2 \rangle_n - \langle |I|^2 \rangle \right)^2 \right\rangle, \tag{8}$$

is the variance of the spectral estimate of the noise calculated at a frequency outside the Doppler peak. We denote the signal-to-noise ratio of this setup SNR_0 and use it as reference when

comparing with the other methods. Assuming that the complex Fourier amplitudes are Gaussian one gets the standard result

$$\frac{\sigma_n^2(N)}{N} = \frac{1}{n}, \tag{9}$$

which was used in Eq. (7).

If we add the two auto spectra for I and Q the signal power will double but the standard deviation of the noise only increase by $\sqrt{2}$. Thus for $\langle |I|^2 \rangle + \langle |Q|^2 \rangle$ we get

$$\mathrm{SNR} = \sqrt{2}\mathrm{SNR}_0, \tag{10}$$

and thereby an improvement in SNR compared to the case only utilizing one of the two detectors by $\sqrt{2}$.

2.2. Auto spectrum of the complex signal

For the auto spectrum of the complex signal the spectral power is

$$\left\langle |I + jQ|^2 \right\rangle = \left\langle |I|^2 + |Q|^2 - jIQ^* + jI^*Q \right\rangle = \begin{cases} 4S + 2N & \text{at Doppler peak} \\ 2N & \text{outside Doppler peak,} \end{cases} \tag{11}$$

where it has been used that $\langle jI^*Q \rangle = -\langle jIQ^* \rangle = S$ at the Doppler peak and 0 outside the Doppler peak.

The uncertainty on the noise level is $\sigma_n(2N)/2N = 1/\sqrt{n}$ because the noise is a sum of n terms each having twice the variance as compared to the situation leading to Eq. (7). The implication is that the signal-to-noise ratio is

$$\mathrm{SNR} = \frac{4S}{\sigma_n\left(2N\right)} = 2S\frac{\sqrt{n}}{N} = 2\mathrm{SNR}_0, \tag{12}$$

which is seen to be twice as good as the signal from one of the individual detectors. This is intuitively not surprising since each detector only receives half of the total signal power in the setup used, but when using the output from both detectors and combing them as a complex signal the full signal power is utilized.

2.3. Cross spectrum

We now turn to the imaginary part of the cross spectrum between I and Q where the spectral power is given as

$$\Im\left(\langle IQ^* \rangle\right) = \begin{cases} \pm S & \text{at Doppler peak} \\ 0 & \text{outside Doppler peak.} \end{cases} \tag{13}$$

Due to the uncorrelated noise sources the average noise power at the output of the cross-spectral analyser is zero. However, we need to estimate the fluctuations around zero in order to use our signal-to-noise definition. We therefore need to estimate $\sigma_n^2(\Im(IQ^*))$ away from the Doppler peak. Here I and Q are uncorrelated Gaussian variables and the product IQ^* will have equal variance of the real and imaginary parts. So,

$$\sigma_n^2\left(\Im\left(IQ^*\right)\right) = \frac{1}{2}\sigma_n^2\left(IQ^*\right). \tag{14}$$

Since the mean of IQ^* is zero we can write the variance (at least for large n) as

$$\sigma_n^2\left(IQ^*\right) = \left\langle |\langle IQ^* \rangle_n|^2 \right\rangle = \frac{1}{n^2}\left\langle |I_1Q_1^* + I_2Q_2^* + \ldots + I_nQ_n^*|^2 \right\rangle. \tag{15}$$

Due to independence all the cross terms in the squared sum will vanish and we are left with n terms of the form $\langle I_k Q_k^* I_k^* Q_k \rangle$. Since the random variables are joint Gaussian and I and Q uncorrelated, this fourth order statistics can, due to Eq. (6), be expanded to products of second order statistics as $\langle I_k Q_k^* I_k^* Q_k \rangle = \langle |I_k|^2 \rangle \langle |Q_k|^2 \rangle = N^2$ (see the Isserlis relation in [7]). Combining these results we get

$$\frac{\sigma_n^2 \left(\Im \left(IQ^* \right) \right)}{N^2} = \frac{1}{2n}, \tag{16}$$

and the signal-to-noise ratio becomes

$$\mathrm{SNR} = \frac{S/N}{1/\sqrt{2n}} = \sqrt{2}\mathrm{SNR}_0. \tag{17}$$

Hence it is seen that the penalty for achieving a flat background spectrum is a reduction in SNR of $\frac{1}{\sqrt{2}}$ relative to that of the auto spectrum of the complex signal.

The results derived in this section are summarized in Table 1 together with the experimental results.

3. Experiments

In order to test the validity of the results derived above two experiments were conducted. First the SNR was measured in the laboratory with the Doppler shift provided by a moving hard target, and secondly on a real atmospheric wind signal.

3.1. SNR from hard target

Figure 3. Schematic drawing of the setup used to measure the SNR from a moving hard target. The neutral density filter (NDF) attenuates the laser beam by 25 dB upon each passage.

The SNR was measured in the laboratory using an experimental setup as shown in Figure 3 and with a telescope with a 1" aperture and 0.10 m focal length. The laser beam was focused weakly on a spinning paper disc adjusted to a relative speed of about 1 m/s and, in order not to saturate the detectors as well as to mimic a real atmospheric return signal, attenuated with a neutral density filter. The filter attenuated the signal by 25 dB upon each passage. The raw signals were sampled at 120 MS/s and processed using a 512 point discrete Fourier transform routine. $n = 4096$ of these spectra were averaged to a single output spectrum resulting in an output rate of approximately 57 Hz. Data was collected for 60 s. Subsequently the laser beam was blocked and another 60 s of data collected. From this the mean backgrounds of the different auto spectra were calculated and the spectra containing Doppler peaks were flattened by dividing with the respective mean background spectra. The SNRs were finally calculated by dividing the value in the bin containing the Doppler peak by the standard deviation of the bins not containing signal.

The results of the measurements are shown in Figure 4 in units of SNR_0 here calculated as the mean SNR of I and Q. First it is noted that there is a slight offset between the SNRs of channels I and Q. This is ascribed to an imbalance in either the optical or electrical part of the

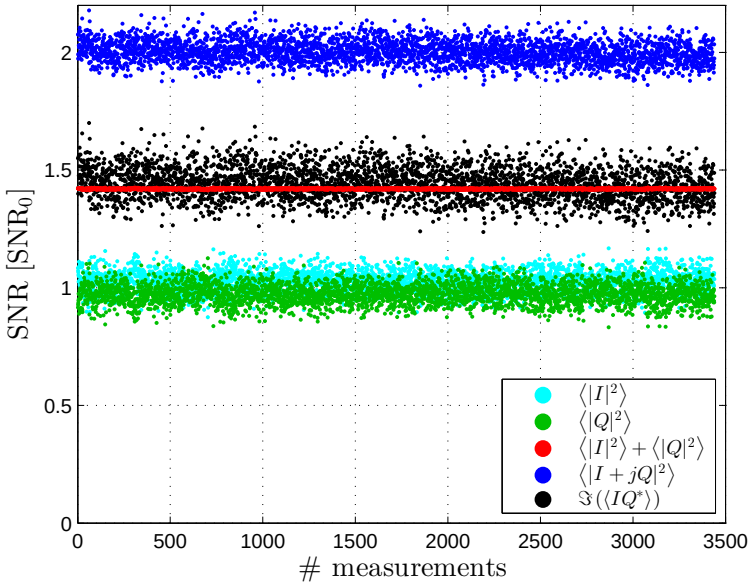

Figure 4. Scatter plot of the measured SNR from a moving hard target and based on the different data processing methods.

system and is the reason for calculating SNR_0 as an average. As predicted by the derivations above the auto spectrum of the complex signal is seen to result in an SNR of two SNR_0 whereas the imaginary part of the cross spectrum only increases the SNR by approximately 1.44 which is very close to the numerical value of $\sqrt{2}$, see Table 1. One distinct feature stand out in the figure and that is that the variance of the $\langle |I|^2 \rangle + \langle |Q|^2 \rangle$ based SNR is much smaller than those of the other four. This is because SNR_0 is calculated as the mean of SNRs of the individual I and Q channels and any further imbalance between the two, e.g. due to changes in the polarisation of the backscattered light during a measurement period, will affect the complex signal and the cross spectrum, but for $\langle |I|^2 \rangle + \langle |Q|^2 \rangle$ they will cancel. The measurement is especially sensitive to changes in the polarisation of the backscattered light because the splitting ratio of the 90°-hybrid is polarisation sensitive, and any instability could therefore lead to the signal not being divided equally between channel I and Q.

3.2. SNR from atmospheric return

For measuring the SNR of the return from the atmosphere the same procedure as for the hard target measurement was used, but this time using a telescope with a 3" aperture, and 0.28 m focal length and with the laser beam focused approximately 80 m from the lidar. The resulting SNR measurements are shown in Figure 5 and the averages of these measurements are shown in Table 1. Although the signal power is expected to have uncertainties due to broadening of the peak because of effects such as speckle broadening and turbulence, good agreement with the theoretical results is again seen; the mean SNR of the complex signal and of the imaginary part of the cross spectrum is 2.01 SNR_0 and 1.41 SNR_0, respectively. In these measurements a sudden drop in the SNR is seen in the end of the time series and these are due to natural variations in the wind speed. When the wind speed approaches 0 m/s the Doppler peak is attenuated by the high pass edge of the bandpass filters with a decreasing SNR as a result. Also a much smaller variance in the measured SNR than for the hard target measurement is seen. red A possible explanation for this could be is the polarisation state of light is better preserved

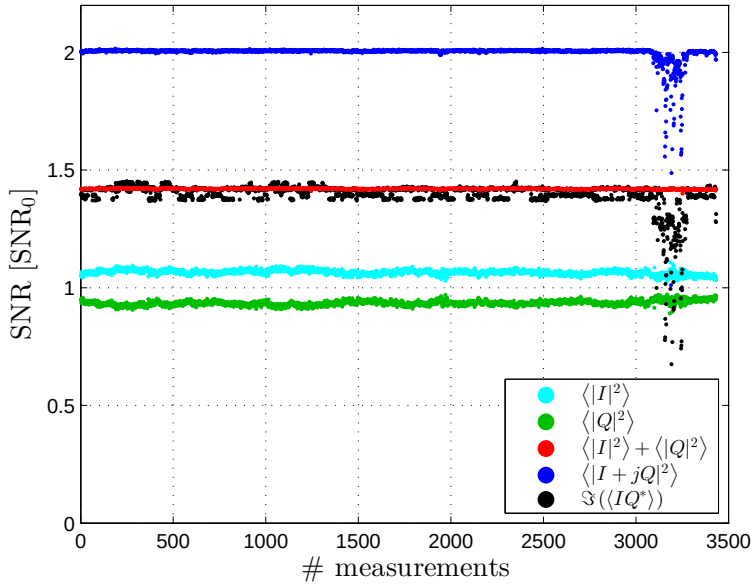

Figure 5. Scatter plot of the measured SNR from an atmospheric return and based on the different data processing methods.

Table 1. SNR/SNR$_0$ for the different data processing methods comparing the theoretically expected values with the experimentally measured values.

	$\langle \lvert I \rvert^2 \rangle$	$\langle \lvert Q \rvert^2 \rangle$	$\langle \lvert I \rvert^2 \rangle + \langle \lvert Q \rvert^2 \rangle$	$\langle \lvert I + jQ \rvert^2 \rangle$	$\Im(\langle IQ^* \rangle)$
Theoretical	1	1	$\sqrt{2}$	2	$\sqrt{2}$
Exp. hard target	1.03	0.97	1.42	2.00	1.44
Exp. atm.	1.07	0.93	1.42	2.01	1.41

in the scattering process with aerosols in the air than with the hard target. However, further investigation is necessary in order to clarify this.

4. Discussion and conclusion

A direction sensing CW lidar has been constructed by incorporating a 90° hybrid into a basic CW lidar setup. The 90° is a completely passive component and requires thus no external control and is less prone to add noise to the measurement as compared to using active components such as an AOM. There are two ways of processing the signals generated by the lidar; calculate either the auto spectrum of the complex signal or the imaginary part of the cross spectrum. The latter method has the very appealing properties of a zero-mean flat background noise spectrum and that all information is contained in the positive half of the spectrum reducing the requirements on data storage. However, we show theoretically and experimentally that these attractive features come at the expense of a reduction in SNR by a factor of $\sqrt{2}$, that is by approximately -1.5 dB. This reduction in SNR will in most situations not limit the operation of the lidar, but under conditions with very clear air or very fast measurements it must be taken into consideration, e.g by increasing the laser output power or perhaps use the auto spectrum of the complex signal instead. Also for Doppler shifts close to zero the auto spectrum of the complex signal may

be advantageous to use because if the Doppler spectrum is perfectly centered around zero the resulting positive and negative peaks of the imaginary part of the cross spectrum will cancel. On the other hand, due to the elimination of the need to normalise the spectrum, necessary for the derivation of accurate wind speeds, the cross-spectral technique does not introduce any estimation error which is inherent to any estimation algorithm. A thorough analysis of the impact on the SNR due to spectral whitening is beyond the scope of this paper and is to be investigated in future a work.

Acknowledgments

This work was supported by "WINDSCANNER - The European ESFRI WindScanner research infrastructure facility" FP7-Infrastructures-2012-1 grant no. 312372.
The resources provided by the Center for Computational Wind Turbine Aerodynamics and Atmospheric Turbulence funded by the Danish Council for Strategic Research grant no. 09-067216 are also acknowledged.
JM would like to thank for the grant provided by the Ingeborg and Leo Dannin foundation.

References

[1] Wagner R, Pedersen T, Courtney M, Antoniou I, Davoust S and Rivera R 2013 *Wind Energy* – ISSN 1099-1824 URL `http://dx.doi.org/10.1002/we.1643`
[2] Bossanyi E, Savini B, Iribas M, Hau M, Fischer B, Schlipf D, van Engelen T, Rossetti M and Carcangiu C E 2012 *Wind Energy* **15** 119–145 ISSN 1099-1824 URL `http://dx.doi.org/10.1002/we.523`
[3] Mann J, Tegtmeier Pedersen A, Dellwik E, Simley E, Abari C F and Mikkelsen T 2014 Experimental demonstration of an image-reject cw coherent doppler lidar *Proc. of ISARS - 17th Int. Symp. for the Advancement of Boundary-Layer Remote Sensing*
[4] Wang C, Gao L, Li Y and Cong H 2009 Investigation of balanced detection and receiver for coherent lidar *Proc. of SPIE - the Int. Society for Optical Engineering* vol 7382 (SPIE) p 7382 0I ISSN 0277-786X
[5] Abari C F, Tegtmeier Pedersen A, Rodrigo P J, Sjöholm M, Peucheret C, Mikkelsen T and Mann J 2014 A homodyne image-reject optical front-end receiver architecture for improved signal detection in coherent doppler lidars *Proc. of ISARS - 17th Int. Symp. for the Advancement of Boundary-Layer Remote Sensing*
[6] Angelou N, Foroughi Abari F, Mann J, Mikkelsen T and Sjöholm M 2012 Challenges in noise removal from doppler spectra acquired by a continuous-wave lidar *Proc. of the 26th Int. Laser Radar Conf.*
[7] Koopmans L 1974 *The spectral analysis of time series* (Academic Press) ISBN 0124192505